Effect of gust and pitch on airfoil lift studied using a discrete vortex simulation

Nitin Chitrala*
North Carolina State University, Raleigh, NC 27695-7910, USA

Yi Tsung Lee†
North Carolina State University, Raleigh, NC 27695-7910, USA

In this paper, we present load analysis of an airfoil experiencing gust using a low-order framework based on Unsteady Thin Airfoil Theory and a Lumped Vortex Element (LVE) method to model unsteady airfoils encountering transverse gusts. An airfoil encountering a transverse gust is known to experience highly unsteady aerodynamic loads. Recent research has proposed utilizing a pitch-down maneuver to mitigate lift spikes that occur in these gust regions. To further explore this proposal, we decided to compare the lift curve of an airfoil going through a region of gust with an airfoil going through a pitch-and-return maneuver in place of the gust region. Because pitch-down maneuvers on an airfoil generate a significant decrease in lift, a superposition of such a pitching maneuver and a gust region will be explored as a method of mitigating gust. In our experiment, we first run a control simulation of an airfoil moving through a region of gust. Secondly, we determine a pitch-up-and-return maneuver with a lift curve that is highly similar to the control lift curve. We then superpose the gust region with a pitch-down-and-return maneuver that has the negative amplitude of the pitch-up-and-return maneuver and run our simulation. The results from our experiment show that within the region where the airfoil is completely exposed to the gust and it is fully pitched down, the lift coefficient of the airfoil is very close to zero. In the regions where the airfoil is partially exposed to the gust or is within the pitching process, the lift is more volatile but can be controlled with careful manipulation of the properties of the pitch-down maneuver. Flowfield imagery and load results show how an additional uniform gust-induced velocity can mostly be mitigated by a simple pitch motion. The extension of this study can focus on more complex gust profiles and the technique of designing the gust mitigation motion.

Nomenclature

a	smoothing parameter
K	non-dimensional pitch rate
x	chordwise coordinate
c	chordwise length
θ	chordwise angular coordinate
α	angle of attack
α_{max}	pitching amplitude
ϕ	velocity potential
Γ	vortex core strength
U_∞	freestream velocity
u	velocity in horizontal(x) direction
w	velocity in vertical(z) direction
w_g	gust velocity
W	downwash velocity
t^*	non dimensional time

*Undergraduate Student, Department of Mechanical and Aerospace Engineering, nachitra@ncsu.edu, Student Member, AIAA
†Ph.D. student, Department of Mechanical and Aerospace Engineering, ylee26@ncsu.edu, Student Member, AIAA

Δt	pitch span
BV	bound vortex
GR	gust ratio
GWC	gust width to chord ratio
FV	free vortex

I. Introduction

Unsteady aerodynamics is a field of study that focuses on the time-dependent flow field property change and the corresponding interactions between the flow field and lifting surfaces. Knowledge in such a field is necessary to understand and model time-dependent phenomena such as flutter (Berci,2021 [1]), vortex-shedding (Shukla et al. 2007 [2]), gust, and a variety of other flow phenomena. Compared to conventional static state aerodynamics, these sudden changes in flow properties can create many unexpected challenges for vehicle control and flight stability. The motivation for the research in the field has recently been boosted thanks to many applications such as the micro-air vehicles (MAVs) operating in gusty conditions (Lueng et al. 2018 [3]. In these applications, the vehicles are much more sensitive to any sudden change in the flow field. As a result, the study of unsteady flow field behavior interacting with lifting surfaces and the mechanism available for mitigating such undesired performance become a critical research topic.

Among many unsteady phenomena, gust has been proved to be one of the most troublesome issues for vehicle stability. Gust refers to a sudden change in velocity within the flow field. When an airplane wing is exposed to a field of gust, it experiences additional induced velocity on the airfoil, changing the effective α, and increasing lift. As a result, a lot of gust mitigation proposals such as the work from Herrmann [4] now work to reduce the increase in lift that occurs when entering the gust region. The earliest gust research dates back to the 1930s when Küssner [5] determined that transverse gusts caused the highest wing stresses compared to gusts acting in other directions. Experimentally, Küssner attributed the effect of this vertical gust to a change in the angle of attack, recording airplane wing deflection during stormy weather. During flight, entering a region of gust momentarily induces additionally velocity along the length of the region of the wing exposed to the gust. This can cause turbulence and further discomfort during flight. The strength of the gust is typically defined with a parameter called gust ratio, GR, which will be further introduced below. This ratio can help quantify the severity of the effect of gust, which can span from slight discomfort to severe structural damage [6].

Following Küssner's observations, an increased emphasis was placed on understanding and mitigating the effects of transverse gusts in later research. Sedky et al. [7] presents three maneuvers which have been used in lift regulation as a means of mitigating gust effects. The first of the three maneuvers is to oppose the induced angle of attack from gust α_{gust} with a pitching angle of attack α such that

$$\alpha_{gust} + \alpha = 0$$

This maneuver assumes fully attached flow and thus does not shed a Leading Edge Vortex (LEV) as shown in the experiments done by Corkery [8] and Andreu-Angulo [9]. The second maneuver is designed such that the total lift response from the superposition of Wagner and Küssner's lift response functions sums to zero. Wagner [10] gives the lift response as a function of angle of attack whereas Küssner gives the lift response of a wing exposed to gust. This maneuver assumes fully attached flows at small angles of attack and thus is ineffective at mitigating strong gusts. The third maneuver uses an unsteady Discrete Vortex Model (DVM) [11] to obtain a wing's pitch kinematics. The velocity field, including the gust effect, is predetermined and is imposed on the wing's control points, bound vortices, and shed vortices within the flow field. LEV and Trailing-Edge Vortex (TEV) shedding are enforced by the Kutta condition at both edges of the airfoil.

This paper uses low-order modeling to test the effectiveness of a pitch-down-and-return maneuver in mitigating the lift effect from gust encounters. The use of low-order modeling in unsteady aerodynamics has gained a lot of traction in recent years, leading to a number of different models capable of analyzing certain flow phenomena. Low-order modeling programs are designed to reduce the time and cost needed to analyze unsteady aerodynamics using computational fluid dynamics (CFD) or experimental procedures by capturing key unsteady flow phenomena without overly complex calculations. To develop such a model, the challenge is to rapidly and accurately capture one of the most important unsteady flow physics: leading edge vortex shedding, and its effect on an airfoil. There have been a lot of attempts on achieving the goal, and among these efforts, the concept of leading-edge suction force, which keeps the flow attached until the suction can no longer support the flow attachment, has gained a lot of interest. Ramesh et al. [12] first proposed a parameter called leading edge suction parameter (LESP) and used it as a parameter within unsteady thin airfoil theory

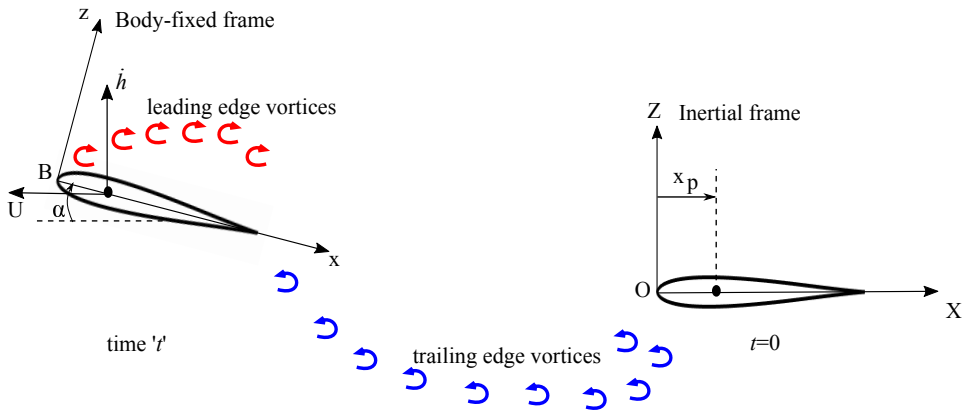

Fig. 1 Illustration of the airfoil kinematics and the discrete vortices shed from it, along with the variables used in the unsteady aerodynamic model

to create a mechanism for predicting LEV shedding initialization and termination. It states that an airfoil at a Reynolds number will have a critical LESP value which it can support regardless of motion kinematics, and as long as the LESP increases above that value the LEV shedding will start. The same concept has been inherited by Narsipur et al. [13, 14] with a Lumped-Vortex Element (LVE) model as the basis for trailing edge separation prediction. A more detailed study on leading edge suction force in CFD has been done in the work of Narsipur et al. [15] and experimentally by Saini et al. [16, 17]. The improvement and modification to increase the low order model's capability has also been done in the work of SureshBabu [18] and Lee et al. [19], where model reduction and a state variable form to couple with structure dynamic equations are investigated. In this paper, we follow the work in Narsipur et al. [14] and add a region of top-hat profile transverse gust (from the work of Corkery et al. [8]). Here, the flow field is simulated as a function of time, and a complete load history is taken for each trial. As a comparison, much like the first gust mitigation method presented in [7], an Eldredge pitch-up-and-return maneuver (Eldredge et al. [20]) can be used to mirror the lift curve of the gust only flowfield. In our model, we can control the three main properties of the Eldredge pitch-and-return motion: K, the non-dimensionalized pitch rate, (a measure of how quickly the pitching maneuver will reach the maximum amplitude of pitch), α_{max}, the pitching amplitude (the maximum α to which the airfoil pitches to), and Δt, the pitch span (the time that the airfoil is at α_{max}). In this paper, we propose that a superposition of a carefully curated Eldredge pitch-down-and-return with gust effect can be used in gust mitigation applications.

The paper will be organized as follows: Sec. II will introduce the basic LVE method and the LESP for the LEV shedding mechanism along with gust implementation to the solver. The following Sec. III demonstrates the results of the superposition method, including flow field imagery, load curves, and quiver plots fit with a gust region. This section also lays out the methodology that was used to find the pitching maneuver that best mitigated lift. Finally, in Sec. IV, we summarize the conclusions from this study.

II. Theory

The schematic representation in figure 1 represents how the discrete vortex method is used to model complex interactions between vortices and airfoil. For an airfoil of chord c undergoing arbitrarily prescribed motion, the motion can be defined by the pitch angle α, the heave position h, and the respective velocities $\dot{\alpha}$ and $\dot{h}$. The pivot point, located at a distance x_p aft of the leading edge, denotes the center of rotation of the airfoil. Two frames are typically defined to be used in the model: Body-fixed frame Bxz consist of a moving origin located on the leading edge and the x and z axes extending in the chord-wise and chord-normal directions and inertial frame will define a universal origin and with X and Z being constant axes. The wake of the airfoil consists of discrete vortices both from the leading edge and the trailing edge to capture the flow field information.

A. Unsteady Aerodynamic Model

The unsteady aerodynamic model used in this work is based on Lumped Vortex Element (LVE) method, Unsteady Thin Airfoil Theory, and Discrete Vortex Method. The LVE states that an airfoil can be represented by several bound

vortex elements concentrated on points along the camberline of the airfoil to represent the bound circulation on the airfoil as a time-dependent variable. The airfoil can be separated into several panels, with each bound vortex located at the quarter-chord position of each panel with the individual strength Γ, and at three quarter-chord position of the panel is defined as a control point. Based on the Unsteady Thin Airfoil Theory, at any time instance, the zero-normal-flow condition needs to be fulfilled following the equations below:

$$(\nabla\phi_B + \nabla\phi_w + \mathbf{U}_0 - \mathbf{U}_{rel} - \dot{\boldsymbol{\alpha}} \times \mathbf{r}) \cdot \mathbf{n} = 0 \tag{1}$$

Here, the $\nabla\phi_B$ is the velocity induced due to the velocity potential from bound vortex elements, while $\nabla\phi_w$ is the velocity induced due to all the wake including LEV and TEV. The $\vec{U}_0$ denotes the free stream velocity vector, $\vec{U}_{rel}$ is the translational velocity of the airfoil, and $\dot{\alpha} \times \vec{r}$ is the velocity induced due to the airfoil pitch motion, where $\dot{\alpha}$ is the pitch angular velocity and $\vec{r}$ is the position vector of a point on the airfoil relative to the pivot point. This equation will be applied to all N control points along the camberline and provide N equations to solve the corresponding unknowns. A more usual form of the equation will then be:

$$\nabla\phi_B \cdot \mathbf{n} = -(\nabla\phi_w + \mathbf{U}_0 - \mathbf{U}_{rel} - \dot{\boldsymbol{\alpha}} \times \mathbf{r}) \cdot \mathbf{n} = -Wn \tag{2}$$

At every time step, this equation can be used to solve for the time-dependent bound vortex strength on each panel, which affects the left-hand side of the equation. The right-hand side can be regarded as the induced downwash normal to the panel and can be solved with all the known flow filed data. The induced velocity calculation from any vortex will follow the typical Biot-Savart law in the form as follows:

$$u_i = \frac{\Gamma_j}{2\pi r_{ij}^2}(z_i - z_j) \tag{3}$$

$$w_i = -\frac{\Gamma_j}{2\pi r_{ij}^2}(x_i - x_j) \tag{4}$$

This equation gives the induced velocity $\vec{u}_i$ at position $\vec{x}_i = (x_i, z_i)$ due to the vortex at $\vec{x}_j = (x_j, z_j)$ with vortex strength Γ_j and the distance between the two point denoted as r_{ij}. With all this information, the final form of the zero normal flow equation is often represented as an influence matrix equation as follows:

$$\begin{bmatrix} a_{11} & a_{12} & \cdots & a_{1N} \\ a_{21} & a_{22} & \cdots & a_{2N} \\ \cdots & \cdots & \cdots & \cdots \\ a_{N1} & a_{N2} & \cdots & a_{NN} \end{bmatrix} \begin{bmatrix} \Gamma_1 \\ \Gamma_2 \\ \cdots \\ \Gamma_N \end{bmatrix} = \begin{bmatrix} -Wn_1 \\ -Wn_2 \\ \cdots \\ -Wn_N \end{bmatrix} \tag{5}$$

where the element a_{ij} indicates the unit normal bound vortex induced velocity on the control point :

$$a_{ij} = \left(\frac{1}{2\pi r_{ij}^2}(z_i - z_j), -\frac{1}{2\pi r_{ij}^2}(x_i - x_J) \right) \cdot \mathbf{n}_i \tag{6}$$

With all the bound vortex strengths being solved at every time step, this information can be used to calculate the aerodynamic load.

B. LESP and discrete vortex shedding

To simulate the unsteady physics, the discrete vortex shedding from the trailing edge at every time step and the accurate prediction of LEV shedding is required. In our current model, the discrete vortex shedding at the trailing edge is achieved by the introduction of new TEV into the influence matrix equation as an additional unknown. The Kelvin condition is used as an additional equation, which takes the form as:

$$\sum \Gamma_b(t - \Delta t) = \sum \Gamma_b(t) + \Gamma_{TEV} + \Gamma_{LEV} \tag{7}$$

With newly added TEV position determined by the work in Narsipur et al. [13], the strength of the new vortex and all the bound vortices can be solved in the influence matrix equation:

$$\begin{bmatrix} a_{11} & a_{12} & \cdots & a_{1N} & a_{1tev} \\ a_{21} & a_{22} & \cdots & a_{2N} & a_{2tev} \\ \cdots & \cdots & \cdots & \cdots & \cdots \\ a_{N1} & a_{N2} & \cdots & a_{NN} & a_{Ntev} \\ 1 & 1 & \cdots & 1 & 1 \end{bmatrix} \begin{bmatrix} \Gamma_1 \\ \Gamma_2 \\ \cdots \\ \Gamma_N \\ \Gamma_{TEV} \end{bmatrix} = \begin{bmatrix} -Wn_1 \\ -Wn_2 \\ \cdots \\ -Wn_N \\ \sum \Gamma_b(t - \Delta t) \end{bmatrix} \tag{8}$$

The LEV shedding prediction can be achieved by adopting the Leading Edge Suction Parameter (LESP) concept from the work of Ramesh et al.[12]. The connection of the bound vortex strength at every step to LESP follows the work from Aggarwal [21], suggesting that the strength of the bound vortex can be used to represent the leading edge suction force.

$$LESP(t) = \frac{1.13(\Gamma_1(t))}{U_\infty(t)c\left[\cos^{-1}(1 - \frac{2l}{c}) + \sin\left(\cos^{-1}(1 - \frac{2l}{c})\right)\right]} \tag{9}$$

For each airfoil at a specific Reynolds number, there exists a constant $LESP_{crit}$, indicating that there is only a limited amount of suction force an airfoil can provide during the unsteady motion. Once the corresponding $LESP$ exceeds this threshold, separation will start from the leading edge and form LEV shedding while the LESP is kept at this critical value. It also indicates that there is a limited strength of Γ_1, so the new influence matrix equation can be formed to solve for not just for a new TEV but also a new LEV simultaneously.

$$\begin{bmatrix} a_{12} & \cdots & a_{1N} & a_{1tev} & a_{1lev} \\ a_{22} & \cdots & a_{2N} & a_{2tev} & a_{2lev} \\ \cdots & \cdots & \cdots & \cdots & \cdots \\ a_{N2} & \cdots & a_{NN} & a_{Ntev} & a_{Nlev} \\ 1 & \cdots & 1 & 1 & 1 \end{bmatrix} \begin{bmatrix} \Gamma_2 \\ \cdots \\ \Gamma_N \\ \Gamma_{TEV} \\ \Gamma_{LEV} \end{bmatrix} = \begin{bmatrix} -Wn_1 \\ -Wn_2 \\ \cdots \\ -Wn_N \\ \sum \Gamma_b(t - \Delta t) \end{bmatrix} - \begin{bmatrix} a_{11} \\ a_{21} \\ \cdots \\ a_{N1} \\ 1 \end{bmatrix} \Gamma_{1,crit} \tag{10}$$

After solving for the strength of the newly created discrete vortex along with the bound vortex strength, the induced velocity for the entire wake can be calculated and used to predict the wake vortex motion in the following steps, which allows us to have a complete flow field simulation at every time step.

C. Transverse Gust effect

The transverse gust effect calculation is achieved by adding the additional gust-induced velocity at any point of interest with the creation of a gust field function. The first modification to the solver is that the right-hand side of the influence matrix equation of each panel will now be:

$$Wn_i = (\mathbf{W}_i + \mathbf{w}_g(\mathbf{x}_i)) \cdot \mathbf{n}_i) \tag{11}$$

where $\vec{W}_i$ is the downwash without gust and $\vec{w}_g(\vec{x}_i)$ is the local gust velocity vector at position x_i. The second modification will be that the velocity of all the free vortices needs to account for this additional gust velocity, so how each vortex maneuver will now be affected in the flow field:

$$\mathbf{u}_{FV} = \mathbf{u}_\infty + \mathbf{u}_{ind,BV} + \mathbf{u}_{ind,FV} + \mathbf{w}_g \tag{12}$$

These two modifications indicate that the gust directly affects the discrete vortex shedding process by affecting the bound vortex strength calculation. The flow field development is also affected due to the additional velocity from the gust moving the vortex away. As a result, the load is also dramatically altered by the introduction of gust.

III. Results

Following the experimental work from Sedky[7], we use our low-order method to simulate a non-pitching airfoil interacting with different levels of gust. Two different strengths of gust are applied to the simulation with $LESP_{crit}$ set at a small value of 0.06 to allow easy LEV shedding in the simulation. This work presents the load prediction of the airfoil moving through a simulation fitted with the superposition of the pitch-down-and-return maneuver and gust region.

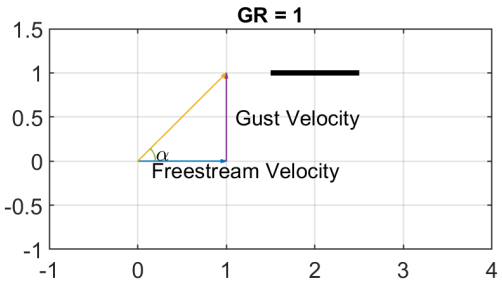

Fig. 2 Illustration of the how to use angle relations to find a good value of α_{max}

A. Gust Region

Gust ratio, GR, is defined as the maximum gust velocity, $v_{g,max}$, relative to the free stream velocity U_∞ following the below definition:

$$GR = \frac{v_{g,max}}{U_\infty} \tag{13}$$

In this work, we choose $GR = .5$ and 1. Although gust can be easily defined as two sections with zero gust and full gust individually, in an actual flow field, there must be a gust velocity gradient near the gust edges to smooth the velocity distribution to the neighboring free stream horizontal velocity. As a result, we use a smooth function inspired by the Eldredge pitch-up and return function[22], to create a gust velocity profile that smooths the velocity distributions at the edge of the gust region and creates a slope to merge the horizontal velocity to the free stream one. The gust velocity distribution can be defined using the following equation:

$$G(x) = \ln\left[\frac{\cosh(a(x-x_1)/c)\cosh(a(x-x_4)/c)}{\cosh(a(x-x_2)/c)\cosh(a(x-x_3)/c)}\right] \tag{14}$$

with a being a smoothing parameter from Granlund et al.[23] to control the smoothing at four turning points of x_1, x_2, x_3 and x_4. The final velocity profile is then defined by

$$w_g(x) = GR \cdot U_\infty \frac{G(x)}{\max(G(x))} \tag{15}$$

In this work, the total gust region width non-dimensionalized by the chord length, GWC, is chosen to be 9.23. This setting means that a gust velocity field with its width being 9.23 times of chord length is moving toward the airfoil, resulting to the airfoil easily being fully exposed to the gust.

B. Eldredge Pitch-and-Return Maneuver

Since the gust region is designed using similar profile from an Eldredge pith-up-and-return motion profile, we propose that the counter-gust motion should also use the same motion to smooth the pitching motion history and to generate a similar lift curve to the case with pure gust effect. The Pitch angle of the motion can be defined using the following equation:

$$G(t) = \ln\left[\frac{\cosh(a(x-t_1)/c)\cosh(a(x-t_4)/c)}{\cosh(a(x-t_2)/c)\cosh(a(x-t_3)/c)}\right] \tag{16}$$

$$\alpha(t) = \alpha_{max}\frac{G(t)}{\max(G(t))} \tag{17}$$

In this expression, the four time instances t_1 to t_4 mark the four turning points of the profile, with t_1 = time of the start of ramp, $t_2 = t_1 + \alpha_{max}/2K$, t_3 = starting time of pitch down, $t_4 = t_3 + \alpha_{max}/2K$, where α_{max} is the maximum pitch up angle and K is the non-dimensional pitch rate. To generate a pitch-up-and-return maneuver with a lift curve that is similar to the plain gust case, t_1, t_3, α_{max} and K, with $\Delta t = t_3 - t_1$ are carefully manipulated to generate the lift curve that is similar to the plain gust case. The non-dimensional pitch rate, K, controls how fast the pitching maneuver moves from $\alpha = 0°$ to α_{max}. Higher value of K results in a quick pitch maneuver and generate a rapid C_l increase. To select a good maximum pitch angle α_{max}, we use angle relations derived from the definition of gust ratio (13) illustrated in figure 2. It considers the combined gust and free-stream together and thus results in a different effective angle of attack

on the airfoil, which is considered to be a good reference angle for the pitching motion. Although it is a good indication of how strong the pitching should be, the number can also be shifted slightly to better mimic the lift peak and curve of the control gust motion. Lastly, we choose a Δt value that allows the airfoil to be pitched down through the entirety of the gust region. To find the minimum time of Δt, we use the following relation:

$$\Delta t_{min} = GWC(1 - 2K_g)c/U_\infty \tag{18}$$

K_g is a term that determines the portion of gust which has not yet reached the full strength at the two slope region. It acts similarly to the pitch rate, K, in that it is the motion which basically governs the slope of the ramp region. In our study, $K_g = 0.2$ is used, meaning that both of the two ramp region, $x_2 - x_1$ and $x_4 - x_3$, each take 20% of the entire gust profile width. As a result, the Δt, which governs the time needed for the airfoil to stay at the peak pitching position, is suspected to be highly related to the K_g, and is thus connected through equation 18. Table 1 below shows the properties that we used to create pitching maneuvers to mitigate gust regions of different strengths.

Table 1 Eldredge Pitch Maneuver Properties

Gust Properties			Eldredge Pitch Properties			
GR	GWC	K_g	α_{max}	K	t_1	Δt
1	9.23	0.2	45°	0.5	1	6.5
0.5	9.23	0.2	28°	0.16	0.2	5.7

As shown in the table, we also manipulate t_1, which is the time of our simulation at which the pitching maneuver begins. We usually attempt to align t_1 with the time at which the airfoil enters the gust region, but when using Eldredge maneuvers with high K, we delay the start of the pitching motion as seen above.

From here, we can find a pitch-down-and-return maneuver that mirrors the lift curve of the aforementioned pitch-up-and-return maneuver, simply by negating the α_{max} of the pitch-up while holding all the other properties the same. Now, we superpose this pitch-down-and-return motion with the gust region and run our simulation, generating load curves and flowfield predictions.

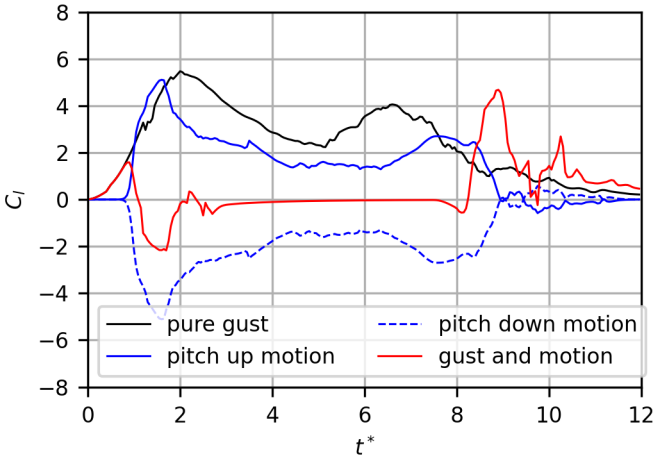

Fig. 3 C_l comparison between pure gust, pitch-up motion, pitch-down motion and Combined gust and pitch-down motion simulation for $GR = 1.0$.

C. Strong Gust Case with $GR = 1$

The lift history is plotted against the non-dimensional time t^* in figure.3, where it can be defined as

$$t^* = tU_\infty/c \tag{19}$$

Our results in Figure 3 show clear gust mitigation between $t^* = 2.5$ and 8 . We see two main lift spikes: one between $t^* = 0$ and 2 and another between $t^* = 8$ and 11. This is further shown in the simulation's flowfield imagery in Figure 4. When lift is close to 0 ($t^* = 3.0, 4.5, 6.0, 7.5, 9.0$), we see that the airfoil is pitched down to α_{max} and is fully within the gust region. Here we see that there is no LEV shedding even despite the large amplitude of the α. During the regions at which the lift spikes, we see heavy LEV shedding. These locations correspond to when the airfoil is not fully submerged in the gust and/or in the midst of of its pitch maneuver. The results, however, do illustrate a steady state result when the airfoil is fully exposed to the max gust velocity and is pitched down to α_{max}, showing the extent of this maneuver's capability of mitigating gust.

D. Medium Gust case with $GR = 0.5$

There is a clear trend that is shown across gust ratios, as shown by our results in Figure 5. Similar to $GR = 1$, our results show clear gust mitigation between $t^* = 2.5$ and 7.5, where the airfoil is pitched down to α_{max} and is fully within the gust region. Again, we see that there is no LEV shedding even despite the large amplitude of the α. Although not as

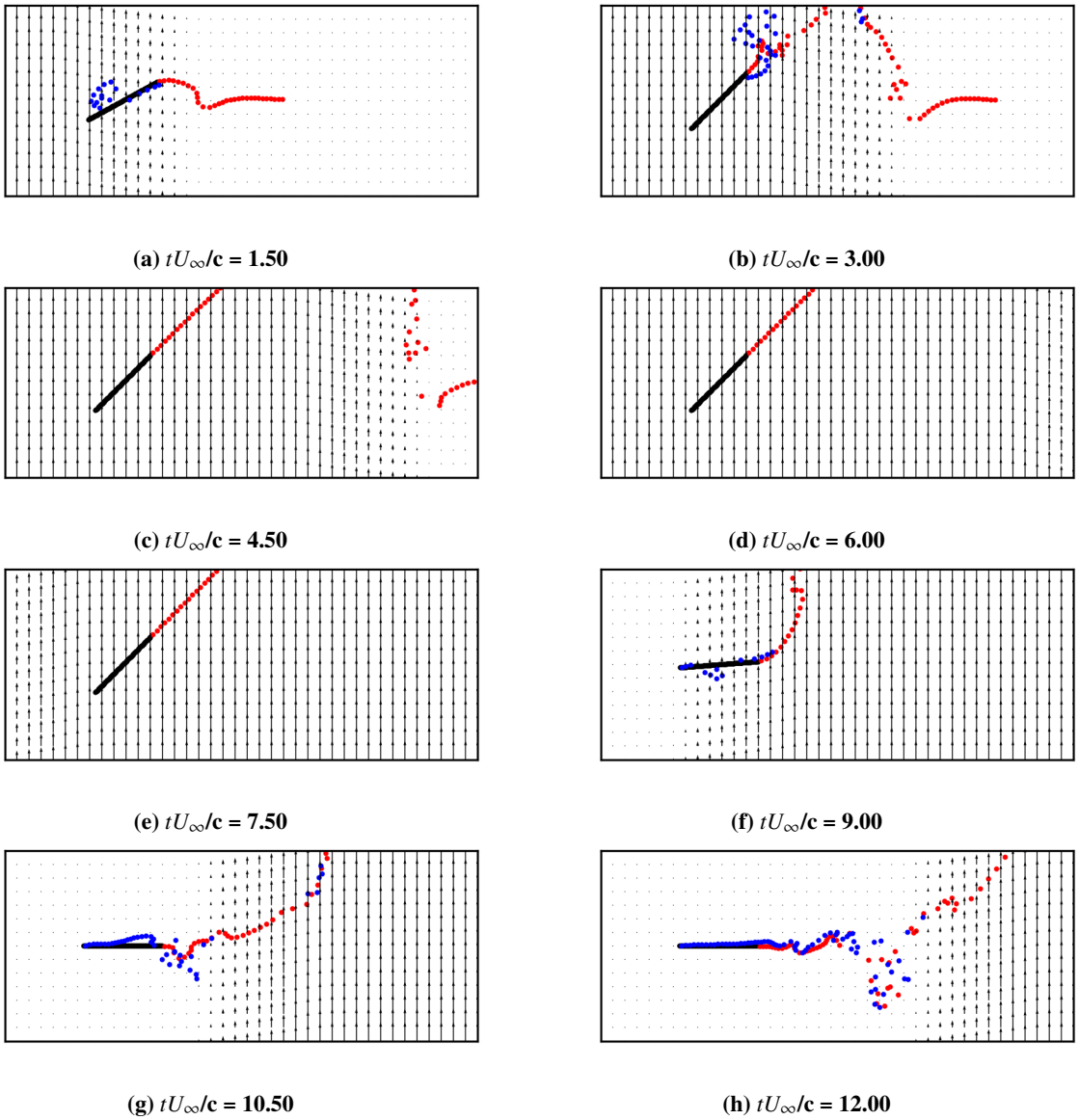

(a) tU_∞**/c = 1.50** **(b)** tU_∞**/c = 3.00**

(c) tU_∞**/c = 4.50** **(d)** tU_∞**/c = 6.00**

(e) tU_∞**/c = 7.50** **(f)** tU_∞**/c = 9.00**

(g) tU_∞**/c = 10.50** **(h)** tU_∞**/c = 12.00**

Fig. 4 Flowfield of $GR = 1$. Red dots are the TEVs and Blue dots are the LEVs.

high as in $GR = 1$, we also see two main lift spikes: one between $t^* = 0$ and 2.5 and another between $t^* = 7.5$ and 10, where the airfoil is not fully submerged in the gust and/or in the midst of of its pitch maneuver. Here, there is heavy LEV shedding. This is illustrated in the simulation's flowfield imagery in Figure 6. The results show clear regions where the lift induced by gust is almost entirely mitigated, regardless of the GR.

In both sets of flowfield imagery (4,6), we see some LEV shedding after the airfoil has moved completely out of the gust region and has returned to $\alpha = 0°$. Typically an airfoil not experiencing any gust effect or undergoing any pitching maneuver will nt shed LEV, but we expect that the cause of this shedding (when $t^* = 10.5$ and 12 for GR=1 and $t^* = 12$ for GR=.5) is due to a combination of the free vortices that are present in the flowfield and the low value of $LESP_{crit}$ that we selected.

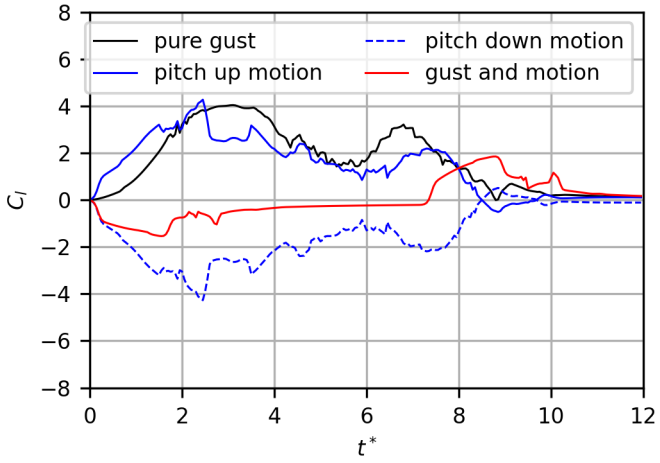

Fig. 5 C_l comparison between pure gust, pitch-up motion, pitch-down motion and Combined gust and pitch-down motion simulation. for $GR = 0.5$

IV. Conclusions and Proposed Work

These results first show the validity of our low-order model as currently constructed. As proposed by [7], our low order model shows that gust effects on an airfoil can indeed be mitigated by a carefully curated pitch maneuver. There is utility in our model, as we are able to conduct various unsteady experiments within the flowfield quickly and efficiently. Our results match the expected results of this experiment. In the future, we will further assess the validity of our model by experimenting with different unsteady flow phenomena.

The results from our low-order simulation with gust implementation show promising results in mitigating the lift spikes caused by gust. We can conclude that this method works especially well for long regions of gust because there will be larger periods of time where the full airfoil is exposed to max gust velocity. We do notice that there are problems with this method when entering and exiting regions of gust, albeit less severe for smaller GR. Further work can focus on decreasing the lift spikes that occur at the exit and entry to the region of gust. Specifically, the effort can focus on finding a more streamlined and universal method to determine the properties of the Eldredge pitch-and-return function which best mimics the lift curve for a chosen GR of any GWC. Effort can also consider other maneuvers such as surge and heave to mitigate gust, especially in the entry and exit regions.

V. Acknowledgements

Both authors thank Dr. Ashok Gopalarathnam and the NCSU Applied Aerodynamics Lab who provided the opportunity and guidance for this project. Nitin Chitrala expresses his gratitude to his co-author, Yi Tsung Lee, who has been a mentor to him. Without him, Chitrala would not be where he was today. Lastly, Chitrala wants to thank his friends and family for their ongoing support in all of his endeavors.

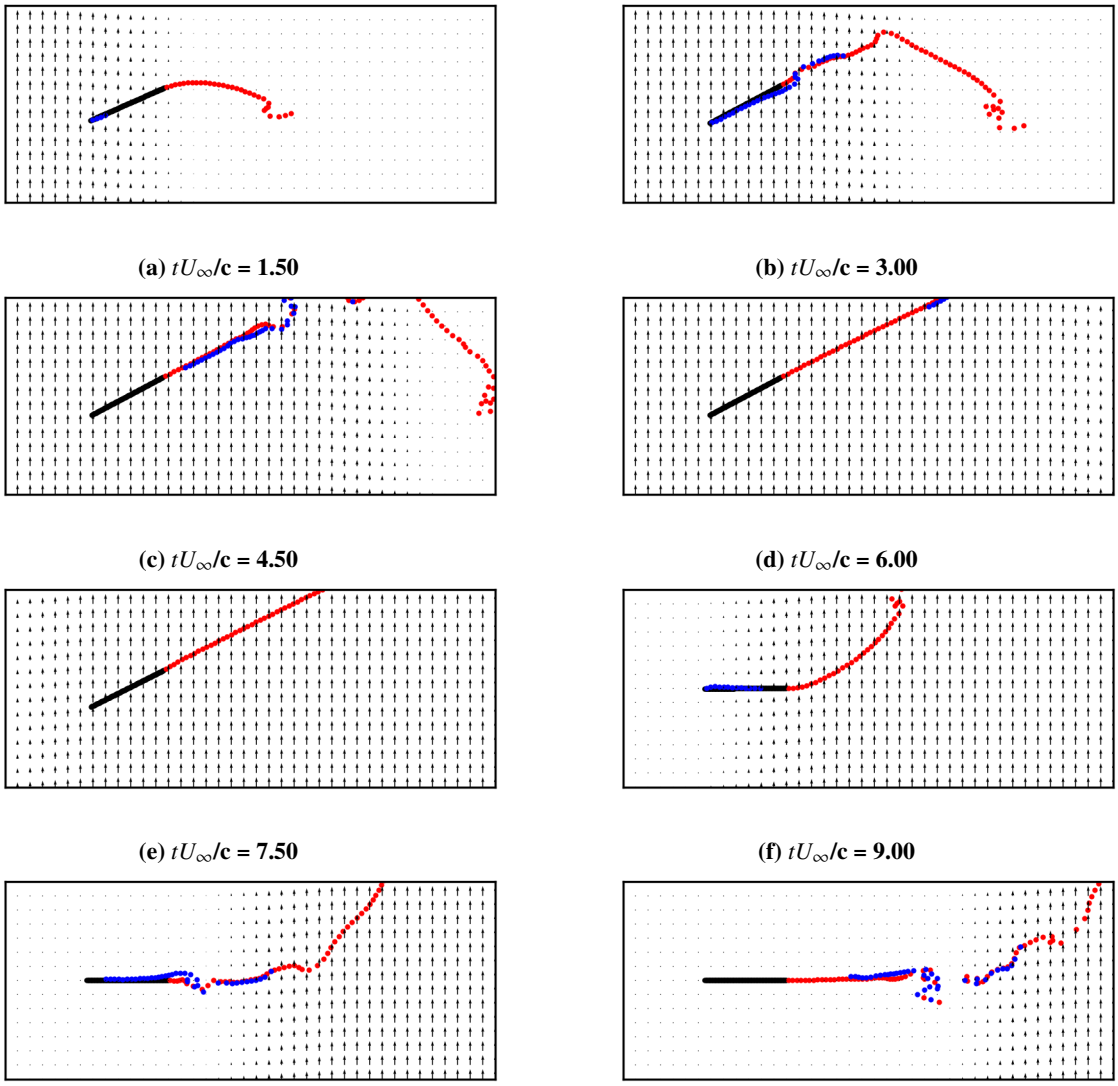

(a) tU_∞**/c = 1.50** **(b)** tU_∞**/c = 3.00**

(c) tU_∞**/c = 4.50** **(d)** tU_∞**/c = 6.00**

(e) tU_∞**/c = 7.50** **(f)** tU_∞**/c = 9.00**

(g) tU_∞**/c = 10.50** **(h)** tU_∞**/c = 12.00**

Fig. 6 Flowfield of GR = 0.5. Red dots are the TEVs and Blue dots are the LEVs.

References

[1] Berci, M., "On Aerodynamic Models for Flutter Analysis: A Systematic Overview and Comparative Assessment," *Applied Mechanics*, Vol. 2, 2021. https://doi.org/10.3390/applmech2030029.

[2] Shukla, R., and Eldredge, J. D., "An inviscid model for vortex shedding from a deforming body," *Theory of Computational Fluid Dynamics*, 2007. https://doi.org/10.1007/s00162-007-0053-2.

[3] Lueng, J. M., Wong, J. G., Weymouth, G. D., and Rival, D. E., "Modeling Transverse Gusts Using Pitching, Plunging, and Surging Airfoil Motions," *AIAA*, Vol. 56, 2018.

[4] Hermann, B., Brunton, P. J. E., Steven L., and Semaan, R., "Gust mitigation through closed-loop control. II. Feedforward and feedback control," *Physical Review Fluids*, Vol. 7, 2022. https://doi.org/10.1103/PhysRevFluids.7.024706.

[5] Küssner, H. G., "Stresses produced in airplane wings by gusts," Tech. Rep. 645, NACA, 1932.

[6] Gudmundsson, S., "Chapter 16 - Performance – Introduction," 2014, pp. 761–789. https://doi.org/10.1016/B978-0-12-397308-5.00016-7.

[7] Sedky, G., Gementzopoulos, A., Andreu-Angulo, I., Lagor, F. D., and Jones, A. R., "Physics of gust response mitigation in open-loop pitching manoeuvres," *Journal of Fluid Mechanics*, Vol. 944, 2022, p. A38. https://doi.org/10.1017/jfm.2022.509.

[8] Corkery, B. H., S. J., and Harvey, J. K., "On the development and early observations from a towing tank-based transverse wing–gust encounter test rig," Vol. 59, No. 9, 2018, p. 135. https://doi.org/10.1007/s00348-018-2586-0.

[9] Andreu-Angulo, B. H. B. H. S. G., I., and Jones, A. R., "Effect of transverse gust velocity profiles," Vol. 58, No. 12, 2020, p. 5123–5133. https://doi.org/10.2514/1.J059665.

[10] Wagner, H., "Über die Entstehung des dynamischen Auftriebes von Tragflügeln," *ZAMM - Journal of Applied Mathematics and Mechanics / Zeitschrift für Angewandte Mathematik und Mechanik*, Vol. 5, No. 1, 1925, pp. 17–35. https://doi.org/10.1002/zamm.19250050103.

[11] Sedky, G., Lagor, F. D., and Jones, A., "Unsteady aerodynamics of lift regulation during a transverse gust encounter," *Physical Review Fluids*, Vol. 5, 2020, p. 074701. https://doi.org/10.1103/PhysRevFluids.5.074701.

[12] Ramesh, K., Gopalarathnam, A., Granlund, K., Ol, M., and Edwards, J., "Discrete-Vortex Method with Novel Shedding Criterion for Unsteady Airfoil Flows with Intermittent Leading-Edge Vortex Shedding," *Journal of Fluid Mechanics*, Vol. 751, 2014, pp. 500–538. https://doi.org/10.1017/jfm.2014.297.

[13] Narsipur, S., Gopalarathnam, A., and Edwards, J. R., "Low-Order Model for Prediction of Trailing-Edge Separation in Unsteady Flow," *AIAA Journal*, Vol. 57, No. 1, 2019, pp. 191–207. https://doi.org/10.2514/1.J057132.

[14] Narsipur, S., Gopalarathnam, A., and Edwards, J. R., "Low-Order Modeling of Dynamic Stall on Airfoils in Incompressible Flow," *AIAA Journal*, 2022, pp. 1–17. https://doi.org/10.2514/1.J061595.

[15] Narsipur, S., Hosangadi, P., Gopalarathnam, A., and Edwards, J. R., "Variation of Leading-Edge Suction during Stall for Unsteady Aerofoil Motions," *Journal of Fluid Mechanics*, Vol. 900, 2020. https://doi.org/10.1017/jfm.2020.467.

[16] Saini, A., and Gopalarathnam, A., "Leading-Edge Flow Sensing for Aerodynamic Parameter Estimation," *AIAA Journal*, Vol. 56, No. 12, 2018, pp. 4706–4718. https://doi.org/10.2514/1.J057327.

[17] Saini, A., Narsipur, S., and Gopalarathnam, A., "Leading-Edge Flow Sensing for Detection of Vortex Shedding from Airfoils in Unsteady Flows," *Physics of Fluids*, Vol. 33, No. 8, 2021, p. 087105. https://doi.org/10.1063/5.0060600.

[18] SureshBabu, A., Ramesh, K., and Gopalarathnam, A., "Model Reduction in Discrete-Vortex Methods for Unsteady Airfoil Flows," *AIAA Journal*, Vol. 57, No. 4, 2019, pp. 1409–1422. https://doi.org/10.2514/1.J057458.

[19] Lee, Y. T., SureshBabu, A., Bryant, M., and Gopalarathnam, A., "State Variable Form of Unsteady Airfoil Aerodynamics with Vortex Shedding," AIAA SCITECH 2022 Forum 2022-1667, 2022. https://doi.org/10.2514/6.2022-1667.

[20] Eldredge, J., Wang, C., and OL, M., "A computational study of a canonical pitch-up, pitch-down Wing Maneuver," *39th AIAA Fluid Dynamics Conference*, Vol. 56, 2009. https://doi.org/10.2514/6.2009-3687.

[21] Aggarwal, S., "An inviscid numerical method for unsteady flows over airfoils and wings to predict the onset of leading edge vortex formation," , 2017.

[22] Eldredge, J. D., and Wang, C., "Low-order phenomenological modeling of leading-edge vortex formation," *Theoretical and Computational Fluid Dynamics*, Vol. 27, 2013, pp. 577–598. https://doi.org/10.1007/s00162-012-0279-5.

[23] Kenneth, G., Ol, M., and Bernal, L., "Experiments on Pitching Plates: Force and Flowfield Measurements at Low Reynolds Numbers," AIAA Paper 2011-0872, https://doi.org/10.2514/6.2011-872, 2011.